Soft Matter

ARTICLE

Effects of resveratrol on the structure and fluidity of lipid bilayers: a membrane biophysical study

A. R. Neves[a], C. Nunes[a], H. Amenitsch[b] and S. Reis[a]*

Resveratrol is a natural active compound whose interest has been increased due to its several pharmacological effects in cancer prevention, cardiovascular protection and neurodegenerative disorders and diabetes treatment. The current work investigates how resveratrol affects membrane order and structure, gathering information determined by X-ray scattering analysis, derivative spectrophotometry, fluorescence quenching and fluorescence anisotropy studies. The results indicate that resveratrol is able to be incorporated into DMPC liposome model systems, either fluidizing or stiffening the bilayer, which largely depends on the membrane fluidity state. These findings suggest that resveratrol effects resemble cholesterol action on biological membranes, thereby contributing to the regulation of cell membrane structure and fluidity, which may influence the activity of transmembrane proteins and hence control the cell signaling pathways. The regulation of a number of cellular functions, thus may contribute to the pharmacological and therapeutic activities of this compound, explaining its pleiotropic action.

Introduction

Resveratrol is a polyphenol compound present in grapes and red wine which has emerged as one of the most promising naturally occurring compounds with a great therapeutic potential in cancer therapy, cardiovascular protection, antioxidant activity, anti-inflammatory action and neuroprotection [1, 2]. The mechanism by which resveratrol exerts such a range of pleiotropic effects is not yet clear [2]. In this respect, it was thought that its action could be directly related to structural and biophysical changes of membranes [3-5]. Indeed, recent evidences suggest that several drugs act through a membrane-lipid therapy, binding to lipids and modulating the structure of membranes, therefore manipulating the behavior and functions of a variety of integral membrane proteins, including ion channels, membrane receptors and enzymes [6, 7]. However, concerning the molecular mechanisms of resveratrol, only few studies have been published so far about its interaction with the lipid membranes and the results are somehow controversial [8-14]. Wesolowska et al. suggested that resveratrol interacted stronger with DMPC and DPPC head group region than with deeper parts of

the bilayer [14]. Similar effects were exerted by resveratrol in other study in DMPC membranes, where the authors proposed resveratrol to be localized near the head group region of the lipid bilayer [11]. However, Selvaraj et al. showed that at higher doses resveratrol localizes within the outer leaflet of the bilayer [12]. Resveratrol-induced decrease of the transition temperature and cooperativity was recorded for DPPC bilayers in Brittes et al. study, which can be interpreted as an increasing membrane fluidity effect [8]. Contrarily, the rigidifying activity of resveratrol on deep portions of POPC:DPPC (1:1) membranes containing 20 mol% cholesterol was also reported by Tsuchiya et al. [13]. Therefore, the correct resveratrol location within the membrane, the effect of this compound on the biophysical properties of the membrane and its effect on the structure of lipid bilayers are questions that require further investigation. For that reason, the objective of the current work was to elucidate the way by which resveratrol affects the membrane order and structure, gathering information at the molecular level on the interaction of this compound with lipid model systems. Hence, large unilamellar liposomes (LUVs) and multilamellar vesicles (MLVs) composed of 1,2-dimyristoyl-*sn*-glycero-3-phosphocholine – DMPC (see Supplementary Fig. 1) were used to mimic cell membranes, since phosphatidylcholines are among the membrane major lipid components and are essential in the regulation of cellular membranes [15]. The accumulation of resveratrol in lipid bilayers was assessed by determining resveratrol partition coefficient by derivative spectrophotometry using liposomes/water systems [16]. The membrane location of resveratrol was studied by fluorescence quenching of probes with well-known, differential and specific location within the bilayer by steady-state and time-resolved measurements [17]. Anisotropy studies were also applied to infer about the effect of resveratrol on lipid order and membrane fluidity [18]. Finally, the structural modifications of the

[a.] UCIBIO, REQUIMTE, Department of Chemical Sciences, Faculty of Pharmacy, University of Porto, Rua de Jorge Viterbo Ferreira, 228, 4050-313 Porto, Portugal.
[b.] Institute of Inorganic Chemistry, Graz University of Technology, Stremayergasse 6/V, 8010 Graz, Austria.

* Corresponding author:
Salette Reis
Department of Chemical Sciences, Faculty of Pharmacy of University of Porto
Rua de Jorge Viterbo Ferreira, 228, 4050-313 Porto, Portugal
TEL: (+351)220428672
FAX: (+351)226093390
E-mail: shreis@ff.up.pt

ARTICLE

Soft Matter

lipid bilayers by the presence of resveratrol were studied by small-angle and wide-angle X-ray scattering [19]. All the experiments were conducted at physiological conditions, such as a buffered pH with adjusted ionic strength similar to the blood plasma conditions (pH 7.4, I = 0.1M) and 37°C, using the biologically active *trans*-resveratrol isomer (see Supplementary Fig. 1).

Results and Discussion

Determination of resveratrol partition coefficient

The partition coefficient of resveratrol was studied in liposome-water instead of the traditional octanol-water system, since it provides a similar environment to the cell membranes, allowing to establish not only hydrophobic, but also electrostatic interactions and hydrogen bonds between resveratrol and the bilayer, due to the amphiphilic nature of the phospholipids [20, 21]. K_p was assessed by UV-Vis derivative spectrophotometry, based on the change of spectral characteristics of resveratrol when it permeates from the aqueous to the lipid phase [16]. Supplementary Figure 2A illustrates the absorption spectra of resveratrol with different concentrations of LUVs of DMPC (pH 7.4, 37°C) and Supplementary Figures 2B and 2C represent the respective first and second-derivative spectra. By using second-derivative spectrophotometry, the effect of background is eliminated and the resolution of the absorption signals is improved by sharpening the bands [22]. Additionally, the derivative spectra exhibit spectral shifts of the λ_{max} with increasing lipid concentrations, indicating that resveratrol partitions from the aqueous to the lipid media [16]. Supplementary Figure 2D shows the best fit of the equation 1 to the second-derivative spectrophotometric data, collected at λ=360 nm, as a function of DMPC concentration. The partition coefficient obtained for resveratrol in LUVs of DMPC at physiological conditions (pH 7.4 and 37 °C) is shown in Table 1, expressed as K_p and log D.
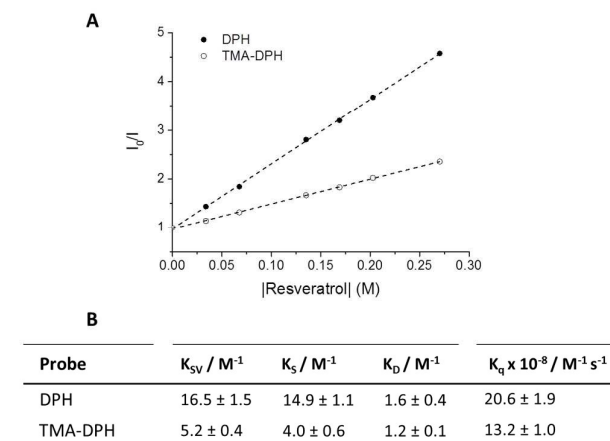
Table 1 – Partition coefficient (expressed as K_p and log D) of resveratrol in LUVs of DMPC at physiological conditions (pH 7.4 and 37 °C).

System	K_p	log D
DMPC	2797 ± 486	3.43 ± 0.14

Note: The values represent the mean ± standard deviation (n = 3).

Resveratrol partition depends on the structure and degree of ionization of the compound and also on the molecular packing of the lipids in the membrane. Therefore, pK_a values and octanol:water partition coefficients for resveratrol were also calculated using Marvin sketch calculator software from Chemaxon[TM]. The calculated value of octanol:water partition coefficient (log $P_{o/w}$) was found to be 3.40 which is very similar to the experimental value of log D (3.43 ± 0.14) obtained at physiological conditions (pH 7.4 and 37°C). The pK_a values determined were 8.49; 9.13 and 10.14 for positions C5; C4' and C3, respectively (see Supplementary Fig. 1). Thus, at pH 7.4, resveratrol is mostly (92%) in its neutral form (correspondent to the protonated hydroxyl groups) what explains the comparable values

Figure 1 – (A) Stern-Volmer plots and (B) values of the Stern-Volmer constant (K_{SV}), static quenching constant (K_S), dynamic quenching constant (K_D) and bimolecular quenching rate constant (K_q) obtained by steady-state fluorescence measurements (I_0/I) of DPH (●) and TMA-DPH (○) in LUVs of DMPC, at physiological conditions (pH 7.4, 37 °C) by increasing concentration of resveratrol. **Note:** All values represent the mean ± standard


| Probe	K_{SV} / M^{-1}	K_S / M^{-1}	K_D / M^{-1}	K_q x 10^{-8} / M^{-1} s^{-1}
DPH	16.5 ± 1.5	14.9 ± 1.1	1.6 ± 0.4	20.6 ± 1.9
TMA-DPH	5.2 ± 0.4	4.0 ± 0.6	1.2 ± 0.1	13.2 ± 1.0

deviation (n = 3).

between the experimental log D in liposome:water system at pH 7.4 and the theoretical log $P_{o/w}$ partition coefficient, since the majority of the existing interactions are hydrophobic forces. Moreover, this result is in agreement with other studies performed in LUVs of DPPC in fluid phase (45°C) and gel phase (25°C), showing values of log D of 3.56 ± 0.4 and 3.38 ± 0.2, respectively [8].

Resveratrol location studies

The membrane location of resveratrol was assessed by steady-state fluorescence quenching and lifetime measurements using DPH and TMA-DPH probes with a known membrane position and depth [23-26].
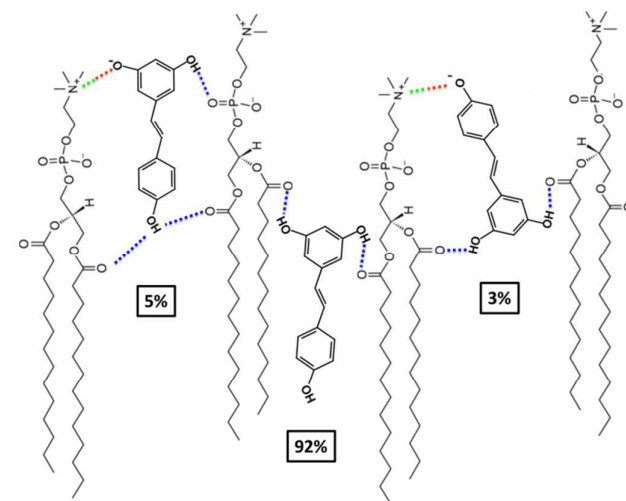
Figure 2 – 2D schematic representation of the orientation and localization of the major microspecies of resveratrol in a DMPC membrane model system, at pH 7.4. **Note:** water molecules are not represented for simplification.
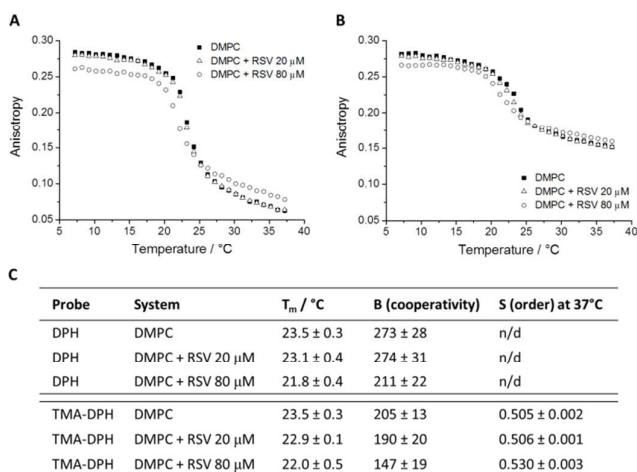
Figure 3 – Steady-state anisotropy of (A) DPH and (B) TMA-DPH as a function of temperature in the absence (■), and in the presence of resveratrol 20 μM (Δ) and 80 μM (○) in DMPC liposomes, at pH 7.4 and (C) respective values of main phase transition temperature (Tm), cooperativity (B), and order (S). **Note:** All values represent the mean ± standard deviation (n = 3). **n/d:** no data with the probe DPH due to the fluidity of the system at 37 °C.

TMA-DPH is reported to be anchored in the phospholipids polar heads and aligned parallel to the acyl chains [23, 26], while DPH is mostly located also aligned parallel to the acyl chains but deeply within the lipid bilayer [24, 25]. The efficiency of resveratrol to quench the fluorophore can be related with its proximity to the probe, therefore providing insights on the location and orientation of the compound inside the membrane. According to this, the quenching of fluorescence was analyzed by the Stern-Volmer plots. As an example, Supplementary Figure 3 shows the excitation and emission spectra of the probe DPH in LUVs of DMPC, in the presence of increasing concentrations of resveratrol (quencher), and the respective Stern-Volmer plots obtained by steady-state fluorescence measurements (I_0/I) and by lifetime fluorescence measurements (τ_0/τ). Similar plots were obtained for the other probe TMA-DPH (See Supplementary Fig. 4), at the same physiological conditions (pH 7.4 and 37°C). In Figures 1A and 1B, one can visualize the Stern-Volmer plots of the two probes simultaneously and the respective slopes corresponding to the Stern-Volmer constants (K_{SV}) of both DPH and TMA-DPH probes, at pH 7.4 and 37°C.

From the analysis of the Figure 1B, it is possible to conclude that the quenching process results mostly from static interactions, once the static quenching constant (K_S) values are much higher than the dynamic quenching constant (K_D) values for both probes, being $K_{SV} \approx K_S$. In addition, the efficiency of the quenching can be assessed by the bimolecular quenching rate constant (K_q) which eliminates the microenvironment surrounding effect of the different probes, allowing the comparison of the two probes [27]. K_q value of DPH probe ($2.1 \pm 0.2 \times 10^9 \ M^{-1} \ s^{-1}$) is higher than that of TMA-DPH probe ($1.3 \pm 0.1 \times 10^9 \ M^{-1} \ s^{-1}$), indicating that resveratrol, at pH 7.4 and 37°C, has a preferential location in a deeper region of the bilayer between the tails of the phospholipids of DMPC, which is in

agreement with other studies [8], but has also some molecules located in the polar head region of the membrane. This result is also in agreement with a previous study with other membrane model systems (EPC, EPC:Cholesterol and EPC:Cholesterol:Sphingomyelin) where resveratrol was able to quench both probes, DPH and TMA-DPH, but the decrease of the probe fluorescence was more pronounced for DPH probe [5]. The membrane location of resveratrol can be correlated with its structure, lipophilicity and also with the degree of ionization of the compound at pH 7.4. According to the pK_a values determined by Marvin sketch calculator software from Chemaxon[TM], at pH 7.4 resveratrol is mostly (92%) in its neutral form what explains the higher fluorescence quenching effect for the deeper region of the membrane. In fact, the neutral form of resveratrol can more easily reach the deepest region of the DMPC bilayer, establishing hydrophobic forces and hydrogen bonds with the tails of the phospholipids (Fig. 2) and leading to the decrease of DPH fluorescence. At this pH, only 8% of the compound is ionized and therefore can stablish electrostatic interactions between its negatively charged hydroxyl groups and the positively charged amine groups present in choline in the polar head region of the phospholipids (Fig. 2), therefore interfering with TMA-DPH fluorescence. Other studies also point to the same conclusions concerning the location of resveratrol in lipid bilayers [28-30]. Koukoulitsa et al. performed molecular dynamics simulations and the results show that molecules that possess phenolic hydroxyl groups orient in the lipid bilayers in an awkward orientation with their long axis such that the majority of the hydroxyl groups anchor in the realm of the head-group. This awkward orientation observed for the hydroxylated molecules maximizes the polar interactions but leaves the remaining hydroxyl group to be embedded in the hydrophobic region [28]. At the same time, Fabris et al. studied the location of resveratrol in DPPC membranes by using EPR measurements. The more marked variations are related with the 7th, 10th and 12th carbon positions, making plausible that the stilbenes compounds are located in this zone of bilayer, in some way anchored to the interfacial or polar region [29]. Ingolfsson et al. also performed molecular dynamics simulations and showed that resveratrol modify bilayer properties by localizing to the interface between the headgroups and the backbone region of the membrane [30].

Resveratrol effect on membrane fluidity

The effect of resveratrol on the membrane fluidity was studied by steady-state fluorescence anisotropy, using DPH and TMA-DPH as probes. In fact, changes in the stiffness of the membrane surrounding the fluorescent probe alter the rotational movement of the probe, thereby promoting changes in the anisotropy.
Figures 3A and 3B show the fluorescence anisotropy of DPH and TMA-DPH in DMPC liposomes as a function of the temperature, in the absence and in the presence of resveratrol, at pH 7.4. From the experimental data displayed, it was possible to calculate the cooperativity (B) and the main phase transition temperature of DMPC (T_m), from the slope and inflection point of the sigmoid curves, respectively. These parameters, along with the order parameter (S) determined at 37°C, are present in Figure 3C.

The analysis of Figure 3C reveals that for DMPC liposomes in the absence of resveratrol, the T_m value of 23.5 ± 0.3°C is consistent with previous reported studies [31-33]. However, T_m decreases 1.5°C in the presence of 80 μM resveratrol, which results in a fluidizing effect for low temperatures range, when the membrane is in the gel phase. However, the effect of resveratrol is just the opposite for temperatures above T_m, resulting in the increase of the anisotropy when the membrane is in the liquid-crystalline phase, what corresponds to the stiffening of the membrane. This effect is more evident in the acyl chain region (given by the probe DPH), but it also happens in the region of the phospholipid heads (given by the TMA-DPH probe) which is also coherent with the above location studies (see Fig. 3). Therefore, the presence of resveratrol increases the order parameter (S) at 37°C in the DMPC membrane, indicating a decrease of the rotational mobility of the probe TMA-DPH. The same parameter could not be calculated for the probe DPH due to the fluidity of the system at 37 °C (Fig. 3C). The cooperativity (B) of the phase transition was significantly reduced by resveratrol, which once again indicates the presence of this compound within the lipid bilayer which is in agreement with other studies [8]. In fact, changes in the cooperativity can be interpreted as an indication of the presence and location of a compound inside the membrane [34].

These effects are only observed with the addition of 80 μM resveratrol, but 20 μM resveratrol did not produce any changes on the temperature dependence of fluorescence anisotropy, probably because the amount of resveratrol intercalated in the lipid bilayer was not sufficient to be translated into a measurable effect. Therefore, these results show that there exists a resveratrol concentration-dependent effect on membrane fluidity and order. Supplementary Fig. 5 summarizes the percentage of fluidization and stiffening effect detected as a function of temperature in the presence of resveratrol 20 μM and 80 μM in DMPC liposomes, at pH 7.4.
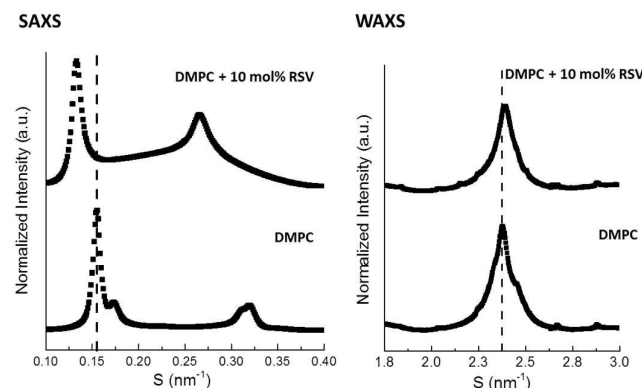
Figure 4 – Small- and wide-angle X-ray diffraction patterns (SAXS and WAXS) of DMPC in the absence and in the presence of 10 mol% of resveratrol at 10°C and pH 7.4.

SAXS and WAXS

In order to study the structural effect of resveratrol on order and packing of DMPC bilayers, SAXS and WAXS measurements were performed at 10, 37 and 45°C. It is well documented that DMPC presents different thermotropic phases depending on the temperature [35, 36]. Hence, below 15°C the gel phase ($L_{β'}$) is formed

where acyl chains are fully extended, tilted and packed in a distorted hexagonal lattice; at 15°C occurs the pre-transition from $L_{β'}$ to the ripple gel phase ($P_{β'}$) where the lipid bilayer is distorted by a periodic ripple; and at 24°C takes place the main phase transition from $P_{β'}$ to the liquid-crystalline phase ($L_α$) where the acyl chains are conformationally disordered [35, 36]. The temperature-dependent X-ray diffraction patterns obtained for SAXS and WAXS of DMPC at pH 7.4 are presented in Supplementary Fig. 6 and the respective long- and short-range distances (d) and correlation lengths ($ξ$) of the first-order Bragg peaks are listed in Table 2.

From the interpretation of the diffraction patterns (see Supplementary Fig. 6) and confronting with the literature data, it is possible to conclude that the lipid dispersion preparation of DMPC at 10°C was still in the ripple phase, probably because the incubation time at low temperature was too short and did not allow the transition to the gel phase that is characteristic at this temperature [37]. Moreover, Tristram-Nagle et al. suggested that the pre-transition from gel to ripple phase of DMPC happens at 13°C [38] and Lewis et al. proposed that, in the case of DMPC, the crystalline phase (L_c), once formed, converts directly into the ripple phase upon heating and this pre-transition is not reversible [39]. Therefore, assuming that we still have a ripple phase at 10°C and a liquid-crystalline phase at 37°C and 45°C, the d values obtained are consistent with previous studies [35, 36, 40]. Thus, the ripple phase has two first-order Bragg peaks with d values of c.a. 65 Å and 57 Å and the liquid-crystalline phase has a d value of c.a. 62 Å (Table 2). Considering the WAXS diffraction patterns, it was already demonstrated that the gel phase presents a pseudohexagonal or orthorhombic chain packing and that the ripple phase shows an hexagonal lattice of the chains [19]. This statement is in agreement with our results (See Supplementary Fig. 6 and Table 2), since the ripple phase has only one diffraction peak with a d value of c.a. 4.2 Å characteristic of the hexagonal chain packing [38, 41] and the liquid-crystalline phase presents a diffuse reflection characteristic of the disordered molten chains of the fluid phase [42].

The addition of resveratrol leads to some changes in the X-ray diffraction patterns of DMPC bilayers at 10°C (Fig. 4 and Table 2).

The first consideration obtained from SAXS is that resveratrol is probably inducing a fluidizing effect of the ripple phase, converting the two first-order Bragg peaks into an only one diffraction peak. Thus, 10 mol% of resveratrol causes an increase of the membrane thickness of DMPC in a total of c.a. 17.5 Å (Table 2), which can be attributed to the loss of the tilt angle. In fact, knowing the length of a DMPC molecule (23.4 Å) and the typical tilt angle of a DMPC bilayer (32.3°), already determined experimentally by Tristram-Nagle et al. [38], it is possible to calculate the contribution of the reduction of the chain tilt to the increase of the membrane thickness in 8.5 Å for each monolayer, i.e. precisely 17 Å in total. Furthermore, the decrease in the correlation length of the DMPC bilayer in the presence of 10 mol% of resveratrol at 10°C is justified by its disturbing effect on the membrane structure, which is indicated by the broader peaks obtained in SAXS diffraction patterns. Concerning the WAXS profile (Fig. 4 and Table 2), the d-spacing is slightly reduced in the presence of 10 mol% of resveratrol probably due to the reduction of the chains tilt angle. The same is not true when the DMPC bilayer is in the fluid phase at 37°C or at 45°C, since resveratrol does not have any significant effect on the

thickness of the bilayer, nor on the distance between the heads of the phospholipids (Supplementary Fig. 7 and Table 2). However, when DMPC is in a more organized state (10°C), resveratrol has a fluidizing effect. This result is consistent with the reported findings obtained with fluorescence anisotropy measurements. Therefore, the results so far indicate that the effect of resveratrol largely depends on the state of membrane fluidity, which shows its influence on regulating the bilayer homeostasis and the tendency towards a relatively stable equilibrium in the structural organization of the membrane.

Experimental
Materials

trans-Resveratrol (> 99% purity) was obtained from Sigma Aldrich (St. Louis, MO, USA) and DMPC was purchased from Avanti Polar Lipids, Inc. (Alabama, USA). The fluorescent probes 1,6-diphenyl-1,3,5-hexatriene (DPH) and 1-(4-trimethylammoniumphenyl)-6-phenyl-1,3,5-hexatriene (TMA-DPH) were supplied by Molecular Probes (Invitrogen Corporation, Carlsbad, California, USA). Resveratrol solutions and lipid suspensions were prepared with phosphate buffer (pH 7.4). For the preparation of phosphate buffer solutions, potassium phosphate monobasic was obtained from Sigma Aldrich and sodium hydroxide from Riedel-de Haën AG (Seelze, Germany). The buffers were prepared using double deionized water from arium water purification system (resistivity > 18 MΩ cm, Sartorius, Goettingen, Germany) and the ionic strength was adjusted to mimic physiological conditions with NaCl (I=0.1 M).

Preparation of DMPC membrane models

Liposomes preparation. LUVs of DMPC were prepared by the classical method of the lipid film hydration, followed by 10 times extrusion process through polycarbonate filters with a pore diameter of 100 nm, at 40°C (well above the main phase transition temperature of the lipid) [43, 44]. For fluorescence measurements, labeled liposomes were prepared by co-dissolving DMPC and the probe (DPH or TMA-DPH) in the organic solvents mixture of chloroform/methanol (3:2, v/v) to give a probe/lipid molar ratio of 1:300. This molar ratio is sufficiently low to ensure the stability of the membrane and its use for drawing conclusions about the location of compounds in biological membranes [45, 46].

Lipid dispersion preparation. Different molar fractions of resveratrol (0, 5 and 10 mol%) were mixed with DMPC in a chloroform/methanol mixture (3:1, v/v). Lipid films were formed by drying the samples under nitrogen stream and left overnight under reduced pressure to remove all traces of the organic solvents. The lipid films were then hydrated with phosphate buffer (pH 7.4) and vortexed, at 40°C for 20 minutes. The lipid dispersions were transferred into glass capillaries of 1.5 mm diameter and the flame-sealed capillaries were stored at 4°C until the X-ray measurements.

Determination of partition coefficient by derivative spectrophotometry

The partition coefficient (K_p) of resveratrol between LUVs suspensions of DMPC and the aqueous buffered solution was determined by derivative spectrophotometry. Resveratrol in phosphate buffer with a final concentration of 20 µM was added to LUVs suspensions with increasing concentrations of DMPC (from 0 to 1000 µM) in a microplate, and incubated in the dark for 30 minutes and 37°C, with agitation. The corresponding reference solutions were identically prepared in the absence of resveratrol. The absorption spectra (250–500 nm range) of samples and reference solutions were recorded at body temperature of 37°C, corresponding to liquid-crystalline phase of DMPC, in a multidetection microplate reader (Synergy HT; Bio-Tek Instruments), accordingly to a well-established protocol [16]. The mathematical treatment of the results was performed using a developed routine, K_p Calculator [16], which (i) subtracts each

Table 2 – Long- and short-range distances (*d*) and correlation lengths (*ξ*) determined from SAXS and WAXS diffraction patterns, respectively, for DMPC in the absence and presence of 10 mol% of resveratrol at 10°C, 37°C and 45°C and pH 7.4.

System	T (°C)	Long distances				Short distances	
		d_1 (Å)	d_2 (Å)	ξ_1 (Å)	ξ_2 (Å)	d (Å)	ξ (Å)
DMPC	10	64.5 ± 0.5	57.3 ± 0.5	697 ± 10	477 ± 10	4.21	47 ± 10
	37	62.3 ± 0.5	-	629 ± 10	-	-	-
	45	61.5 ± 0.5	-	567 ± 10	-	-	-
DMPC + 10 mol% RSV	10	74.8 ± 0.5	-	618 ± 10	-	4.18	54 ± 10
	37	63.3 ± 0.5	-	602 ± 10	-	-	-
	45	63.4 ± 0.5	-	554 ± 10	-	-	-

ARTICLE   **Soft Matter**

reference spectrum from the correspondent sample spectrum to obtain corrected absorption spectra, (ii) determines the second and third derivative spectra in order to eliminate the spectral interferences due to light scattered by the lipid vesicles and to enhance the ability to detect minor spectral features and improve the resolution of bands, and (iii) calculates the K_p value by plotting the second or third derivative spectra values at wavelengths where the scattering is eliminated versus the DMPC concentration [16]. After that, a non-linear least-squares regression method is applied by fitting the following equation to the plot, where K_p is the adjustable parameter:

$$D_T = D_w + \frac{(D_m - D_w)\, K_p\, [L]\, V_\emptyset}{1 + K_p\, [L]\, V_\emptyset} \tag{1}$$

In this equation, D is the second or third derivative intensities obtained from the absorbance values of resveratrol: D_T refers to the total amount of resveratrol, D_w corresponds to resveratrol distributed in the aqueous phase, and D_m corresponds to resveratrol distributed on the lipid membrane phase; K_p is the partition coefficient of resveratrol; $[L]$ is the molar concentration of DMPC; and $V_\emptyset$ is the lipid molar volume of DMPC (0.66 L mol^{-1}).

Membrane location studies by fluorescence quenching

Quenching studies, including fluorescence steady-state and fluorescence time-resolved measurements, were performed by incubating increasing concentrations of resveratrol (from 0 to 80 µM) with DPH and TMA-DPH labeled liposomes with a fixed concentration of DMPC (500 µM), in phosphate buffer (pH 7.4). Samples were incubated in the dark for 30 minutes so that resveratrol could reach the partition equilibrium between the lipid membranes and the aqueous medium, at physiological temperature (37°C).

Fluorescence measurements were carried out at 37°C with excitation/emission wavelengths of 357/429 nm and 361/427 nm for DPH and TMA-DPH, respectively. Fluorescence steady-state measurements were performed in a Jasco FP6500 steady-state spectrofluorimeter equipped with a constant temperature cell holder. All data were recorded in a 1 cm path length cuvette. Fluorescence emission intensity values were corrected for inner filter effects at the excitation wavelength [47]. Fluorescence time-resolved measurements were performed in a Fluorolog Tau-3 Lifetime system. Modulation frequencies were acquired between 10 and 150 MHz and the integration time was 8 s. Manual slits were 0.7 mm, slits for excitation monochromator were 7.0 mm (side entrance) and 0.7 mm (side exit) and for emission monochromator were 7.0 mm (side entrance) and 7.0 mm (side exit). The fluorescence emission was detected with a 90° scattering geometry. All measurements used Ludox as a reference standard (τ=0.00 ns).

The capacity of resveratrol to quench the fluorescence of DPH and TMA-DPH probes was evaluated by determination of the Stern–Volmer constant (K_{SV}) from the slope of the Stern–Volmer plots obtained by steady-state fluorescence measurements (I_0/I) versus the quencher concentration ([Q]) [17].

$$\frac{I_0}{I} = 1 + K_{SV}\,[Q] \tag{2}$$

Two quenching processes can usually be encountered, namely dynamic (collisional) quenching and static (complex formation) quenching. Collisional quenching occurs when the excited fluorophore experiences contact with a molecule that can facilitate transitions to the ground state [27]. Static quenching occurs when the fluorophore forms a stable complex with a molecule in the ground state. In order to study if the quenching mechanism was static or dynamic, the dynamic quenching constant (K_D) was determined from the slope of the Stern-Vomer plots obtained by lifetime fluorescence measurements (τ_0/τ) versus the quencher concentration ([Q]) [17].

$$\frac{\tau_0}{\tau} = 1 + K_D\,[Q] \tag{3}$$

The static quenching constant (K_S) was also determined from the following relation between the K_{SV} and K_D constants.

$$K_{SV} = K_S + K_D \tag{4}$$

In addition, it was possible to calculate the bimolecular quenching rate constant (K_q).

$$K_q = \frac{K_{SV}}{\tau_0} \tag{5}$$

In this equation, τ_0 is the fluorescence lifetime of the probes DPH or TMA-DPH in LUVs of DMPC that were experimentally measured in the absence of the quencher resveratrol. Thus, τ_0 was 7.97 ns for DPH and 3.91 ns for TMA-DPH. K_q constitutes a fundamental parameter to predict the location of resveratrol in the membrane, since the effect of the different microenvironment surrounding the different probes is eliminated [27].

Membrane fluidity studies by fluorescence anisotropy

The effect of resveratrol on the membrane fluidity, main phase transition temperature, phase transition cooperativity and order was studied by fluorescence anisotropy, using DPH and TMA-DPH probes. A fixed concentration of labeled liposomes of DMPC (500 µM) was incubated with different concentrations of resveratrol (0, 20 and 80 µM), followed by 30 minutes of incubation in the dark, at physiological temperature (37°C). The measurements were performed in a Jasco FP6500 steady-state spectrofluorimeter. The excitation/emission wavelengths were set to 357/429 nm and 361/427 nm for DPH and TMA-DPH, respectively. The fluorescence anisotropy was recorded at several temperatures between 7°C and 37°C, by intervals of 1°C. The results obtained in the presence and absence of resveratrol were plotted as steady-state anisotropy (r_s) versus temperature (T) and data was fitted using a sigmoid curve [48, 49].

$$r_s = r_{s_1} + p_1 T \frac{r_{s_2} - r_{s_1} + p_2 T - p_1 T}{1 + 10^{B\left(\frac{1}{T} - \frac{1}{T_m}\right)}} \tag{6}$$

In this equation, p_1 and p_2 correspond to the slopes of the straight lines at the beginning and at the end of the plots and r_{s_1} and r_{s_2} are the respective steady-state anisotropy intercepting values at the y

axis. It was possible to calculate the cooperativity (*B*) and the main phase transition temperature (*T*$_m$) of DMPC, from the slope and the inflection point of the data fitted to sigmoid curves, respectively. The order parameter (*S*) was also calculated through the equation:

$$S = \sqrt{r_\infty/r_0} \qquad (7)$$

where r_0 is the fluorescence anisotropy in the absence of any rotational motion of the probe and r_∞ reflects the restriction of probe motion in each particular membrane system [49, 50]. r_∞ can be calculated from r_s values using the following relationship [51]:

$$r_\infty = {}^4\!/_3\, r_s - 0.10 \quad \text{for} \quad 0.13 < r_s < 0.28 \qquad (8)$$

Small- and wide-angle X-ray scattering

Small-angle X-ray scattering (SAXS) and wide-angle X-ray scattering (WAXS) experiments were performed at the Austrian SAXS beamline in the electron storage ring Elettra (Trieste, Italy) with a monochromatic radiation of wavelength 0.154 nm [52]. The SAXS detector Pilatus3 1M (Dectris, Baden Switzerland) was calibrated using silver behenate powder (*d*-spacing =58.376 Å) [53] and WAXS detector Pilatus 100K (Dectris, Baden Switzerland) with p-bromo benzoic acid with the *d*-spacings taken from Ohkura et al. [54]. Static measurements were taken below (10°C) and above (37°C and 45°C) the main transition temperature of DMPC using a custom made sample cell with a water bath Unistat (Huber, Offenburg, Germany) for cooling. Each diffraction pattern was presented as described in previous works [19, 41], by plotting the normalized scattering intensity in arbitrary units versus the reciprocal spacing (*s*) in nm^{-1}.

$$s = \frac{2\,\sin\theta}{\lambda} \qquad (9)$$

where θ is the diffraction angle and λ is the X-ray wavelength. The diffraction peaks obtained were fitted with Lorentzians, and the positions of maximum intensities and the full widths at half maximum were determined and used to calculate the bilayer distances and the correlation lengths of the lipid bilayers, respectively. Hence, from the peak maximum positions (*s*) of the wide- and small-angle diffraction patterns, the lipid bilayer distances (*d*) were calculated:

$$d = \frac{1}{s} \qquad (10)$$

and the correlation lengths (ξ) of the lipid bilayers were determined from full width at half maximum (*w*):

$$\xi = \frac{2\pi}{w} \qquad (11)$$

Conclusions

Despite the known therapeutic effects of resveratrol, its mechanism of action is still uncertain and this study aimed to bring a new membrane approach to interpret the pleiotropic actions of this compound at a molecular level. The literature review showed some controversial results in this field, presenting contradictory effects of

resveratrol inserted in different membrane model systems [8-14]. In the present study, the results indicate that resveratrol is able to be incorporated into lipid membrane models, suggesting that this compound penetrates into the acyl membrane region but also positions its polar hydroxyl groups near the head group region of the membrane (Fig. 2). Results obtained by anisotropy and X-ray studies indicate that resveratrol has a membrane fluidizing effect for low temperatures, when the membrane is in the gel phase. However, the effect of resveratrol is just the opposite for temperatures above *T*$_m$, resulting in the increase of the anisotropy when the membrane is in the liquid-crystalline phase, what corresponds to the stiffening of the membrane. Therefore, the main conclusion of this study is that resveratrol interaction with biological membranes is dependent on the initial state of the bilayer fluidity. Resveratrol either fluidizes or stiffens the membrane, depending on its initial organizational state and order. This finding seems to justify the contradictory results of the previous studies, as reported in the introduction section. In fact, depending on the membrane model systems used, the lipid compositions are also different, especially in what concerns the degree of unsaturation of fatty acids, the acyl chain lengths, and the head groups of the phospholipids. It seems like membranes in a gel phase are more difficult to permeate by resveratrol and therefore the compound will localize more superficially, causing fluidization of the membrane. On the other hand, if the bilayer is in a fluid state, resveratrol penetrates more easily, being located in a deeper region of the membrane, thereby promoting the structural organization. Thus, resveratrol appears to harmonize the membrane properties, in order to balance and regulate the bilayer structure and order, and consequently its function in the cells, thus contributing to the membrane homeostasis. This effect reminds us the ambivalent role of cholesterol. Indeed, several studies indicate the strong membrane stabilizing effect of cholesterol and its ability to modulate the physicochemical properties of cellular membranes [55, 56]. It has been shown that cholesterol has different effects on membrane fluidity at different temperatures. The sterol reduces membrane fluidity at moderate temperatures (above the *T*$_m$), restraining the movement of phospholipids hydrocarbon chains; but at low temperatures (below the *T*$_m$) cholesterol increases the fluidity of the membrane by disrupting the regular packing of phospholipids and hindering solidification [56, 57]. As a result, resveratrol resembles cholesterol in lipid bilayers, particularly by its membrane stabilizing effect and its ability to modulate the membrane fluidity and cell membrane homeostasis. Consequently, resveratrol may be involved in controlling the activity of transmembrane proteins and hence the cell signaling. Actually, membrane fluidity affects a number of cellular functions, since the activity of membrane proteins is modulated by the surrounding lipid environment [3, 7].
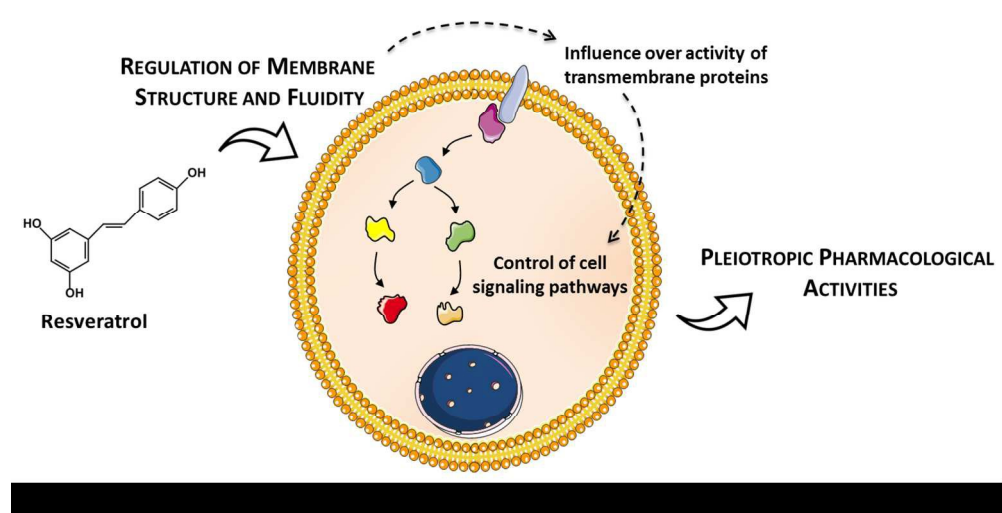
Acknowledgements

References

1. A. R. Neves, M. Lucio, J. L. Lima and S. Reis, *Curr Med Chem*, 2012, **19**, 1663-1681.

2. J. A. Baur and D. A. Sinclair, *Nat Rev Drug Discov*, 2006, **5**, 493-506.

3. D. Delmas and H. Y. Lin, *Mol Nutr Food Res*, 2011, **55**, 1142-1153.

4. A. R. Neves, C. Nunes and S. Reis, *Biochimica et biophysica acta*, 2015, **1858**, 12-18.

5. A. R. Neves, C. Nunes and S. Reis, *The journal of physical chemistry. B*, 2015, **119**, 11664-11672.

6. P. V. Escriba and G. L. Nicolson, *Biochimica et biophysica acta*, 2014, **1838**, 1449-1450.

7. M. Ibarguren, D. J. Lopez and P. V. Escriba, *Biochimica et biophysica acta*, 2014, **1838**, 1518-1528.

8. J. Brittes, M. Lucio, C. Nunes, J. L. Lima and S. Reis, *Chem Phys Lipids*, 2010, **163**, 747-754.

9. J. Garcia-Garcia, V. Micol, A. de Godos and J. C. Gomez-Fernandez, *Arch Biochem Biophys*, 1999, **372**, 382-388.

10. B. Olas and H. Holmsen, *Food Chem Toxicol*, 2012, **50**, 4028-4034.

11. M. G. Sarpietro, C. Spatafora, C. Tringali, D. Micieli and F. Castelli, *J Agric Food Chem*, 2007, **55**, 3720-3728.

12. S. Selvaraj, A. Mohan, S. Narayanan, S. Sethuraman and U. M. Krishnan, *J Med Chem*, 2013, **56**, 970-981.

13. H. Tsuchiya, M. Nagayama, T. Tanaka, M. Furusawa, M. Kashimata and H. Takeuchi, *Biofactors*, 2002, **16**, 45-56.

14. O. Wesolowska, M. Kuzdzal, J. Strancar and K. Michalak, *Biochimica et biophysica acta*, 2009, **1788**, 1851-1860.

15. P. V. Escriba, J. M. Gonzalez-Ros, F. M. Goni, P. K. Kinnunen, L. Vigh, L. Sanchez-Magraner, A. M. Fernandez, X. Busquets, I. Horvath and G. Barcelo-Coblijn, *Journal of cellular and molecular medicine*, 2008, **12**, 829-875.

16. L. M. Magalhaes, C. Nunes, M. Lucio, M. A. Segundo, S. Reis and J. L. Lima, *Nat Protoc*, 2010, **5**, 1823-1830.

17. M. Lúcio, C. Nunes, D. Gaspar, K. Gołębska, M. Wisniewski, J. L. F. C. Lima, G. Brezesinski and S. Reis, *Chemical Physics Letters*, 2009, **471**, 300-309.

18. M. Lucio, H. Ferreira, J. Lima, C. Matos, B. de Castro and S. Reis, *Physical Chemistry Chemical Physics*, 2004, **6**, 1493-1498.

19. C. Nunes, G. Brezesinski, J. L. F. C. Lima, S. Reis and M. Lucio, *Soft Matter*, 2011, **7**, 3002-3010.

20. R. Gulaboski, F. Borges, C. M. Pereira, M. N. Cordeiro, J. Garrido and A. F. Silva, *Comb Chem High Throughput Screen*, 2007, **10**, 514-526.

21. C. Giaginis and A. Tsantili-Kakoulidou, *J Pharm Sci*, 2008, **97**, 2984-3004.

22. N. C. Santos, M. Prieto and M. A. Castanho, *Biochimica et biophysica acta*, 2003, **1612**, 123-135.

23. S. C. Nelson, S. K. Neeley, E. D. Melonakos, J. D. Bell and D. D. Busath, *BMC biophysics*, 2012, **5**, 5.

24. S. Wang, J. M. Beechem, E. Gratton and M. Glaser, *Biochemistry*, 1991, **30**, 5565-5572.

25. R. D. Kaiser and E. London, *Biochemistry*, 1998, **37**, 8180-8190.

26. D. Illinger, G. Duportail, Y. Mely, N. Poirelmorales, D. Gerard and J. G. Kuhry, *Biochimica Et Biophysica Acta-Biomembranes*, 1995, **1239**, 58-66.

27. J. R. Lakowicz, *Principles of Fluorescence Spectroscopy*, Springer, New York, 2006.

28. C. Koukoulitsa, S. Durdagi, E. Siapi, C. Villalonga-Barber, X. Alexi, B. R. Steele, M. Micha-Screttas, M. N. Alexis, A. Tsantili-Kakoulidou and T. Mavromoustakos, *European biophysics journal : EBJ*, 2011, **40**, 865-875.

29. S. Fabris, F. Momo, G. Ravagnan and R. Stevanato, *Biophysical Chemistry*, 2008, **135**, 76-83.

30. H. I. Ingolfsson, P. Thakur, K. F. Herold, E. A. Hobart, N. B. Ramsey, X. Periole, D. H. de Jong, M. Zwama, D. Yilmaz, K. Hall, T. Maretzky, H. C. Hemmings, Jr., C.

Blobel, S. J. Marrink, A. Kocer, J. T. Sack and O. S. Andersen, *ACS Chem Biol*, 2014, **9**, 1788-1798.

31. O. Enders, A. Ngezahayo, M. Wiechmann, F. Leisten and H. A. Kolb, *Biophysical journal*, 2004, **87**, 2522-2531.

32. M. Kozak, A. Wypych, K. Szpotkowski, S. Jurga and A. Skrzypczak, *Journal of Non-Crystalline Solids*, 2010, **356**, 747-753.

33. R. Koynova and M. Caffrey, *Biochimica Et Biophysica Acta-Biomembranes*, 2001, **1513**, 82-82.

34. C. Nunes, G. Brezesinski, C. Pereira-Leite, J. L. F. C. Lima, S. Reis and M. Lucio, *Langmuir*, 2011, **27**, 10847-10858.

35. J. Eisenblätter and R. Winter, *Biophysical journal*, 2006, **90**, 956-966.

36. M. Pinheiro, C. Nunes, J. M. Caio, C. Moiteiro, G. Brezesinski and S. Reis, *Int J Pharm*, 2013, **453**, 560-568.

37. D. Pentak, *Thermochimica Acta*, 2014, **584**, 36-44.

38. S. Tristram-Nagle, Y. F. Liu, J. Legleiter and J. F. Nagle, *Biophysical journal*, 2002, **83**, 3324-3335.

39. R. N. A. H. Lewis, Y.-P. Zhang and R. N. McElhaney, *Biochimica et Biophysica Acta (BBA) - Biomembranes*, 2005, **1668**, 203-214.

40. M. Pinheiro, C. Nunes, J. M. Caio, C. Moiteiro, M. Lucio, G. Brezesinski and S. Reis, *The journal of physical chemistry. B*, 2013, **117**, 6187-6193.

41. C. Nunes, G. Brezesinski, J. L. F. C. Lima, S. Reis and M. Lucio, *Journal of Physical Chemistry B*, 2011, **115**, 8024-8032.

42. A. M. S. Cardoso, S. Trabulo, A. L. Cardoso, A. Lorents, C. M. Morais, P. Gomes, C. Nunes, M. Lúcio, S. Reis, K. Padari, M. Pooga, M. C. Pedroso de Lima and A. S. Jurado, *Biochimica et Biophysica Acta (BBA) - Biomembranes*, 2012, **1818**, 877-888.

43. D. D. Lasic and D. Needham, *Chemical Reviews*, 1995, **95**, 2601-2628.

44. M. J. Hope, M. B. Bally, G. Webb and P. R. Cullis, *Biochimica et biophysica acta*, 1985, **812**, 55-65.

45. D. D. Lasic, *Liposomes - from Physics to Applications*, Elsevier, New York, 1993.

46. M. Lucio, H. Ferreira, J. L. Lima and S. Reis, *Redox report : communications in free radical research*, 2008, **13**, 225-236.

47. A. Coutinho and M. Prieto, *J Chem Educ*, 1993, **70**, 425.

48. J. L. Vazquez, M. T. Montero, S. Merino, O. Domenech, M. Berlanga, M. Vinas and J. Hernandez-Borrell, *Langmuir*, 2001, **17**, 1009-1014.

49. A. Grancelli, A. Morros, M. E. Cabanas, O. Domenech, S. Merino, J. L. Vazquez, M. T. Montero, M. Vinas and J. Hernandez-Borrell, *Langmuir*, 2002, **18**, 9177-9182.

50. W. J. Van Blitterswijk, R. P. Van Hoeven and B. W. Van der Meer, *Biochimica et biophysica acta*, 1981, **644**, 323-332.

51. H. Pottel, W. van der Meer and W. Herreman, *Biochimica et Biophysica Acta (BBA) - Biomembranes*, 1983, **730**, 181-186.

52. H. Amenitsch, S. Bernstorff, M. Kriechbaum, D. Lombardo, H. Mio, M. Rappolt and P. Laggner, *Journal of Applied Crystallography*, 1997, **30**, 872-876.

53. T. N. Blanton, T. C. Huang, H. Toraya, C. R. Hubbard, S. B. Robie, D. Louer, H. E. Gobel, G. Will, R. Gilles and T. Raftery, *Powder Diffraction*, 1995, **10**, 91-95.

54. K. Ohkura, S. Kashino and M. Haisa, *Bulletin of the Chemical Society of Japan* 1972, **45**, 2651–2653.

55. A. Arora, T. M. Byrem, M. G. Nair and G. M. Strasburg, *Arch Biochem Biophys*, 2000, **373**, 102-109.

56. H. Ohvo-Rekila, B. Ramstedt, P. Leppimaki and J. P. Slotte, *Prog Lipid Res*, 2002, **41**, 66-97.

57. R. A. Demel and B. De Kruyff, *Biochimica et biophysica acta*, 1976, **457**, 109-132.

250x127mm (150 x 150 DPI)